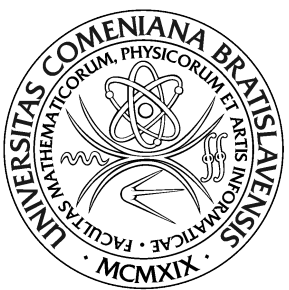


UNIVERZITA KOMENSKÉHO V BRATISLAVE  
FAKULTA MATEMATIKY, FYZIKY A INFORMATIKY



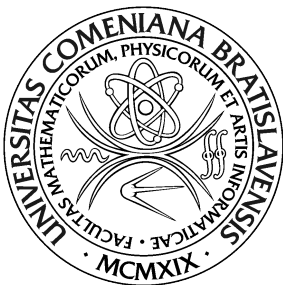
NA EFEKTÍVNE KONŠTRUOVANIE TRACKLETOV OBJEKTOV VE

Diplomová práca

2017

Bc. Stanislav Krajčovič

UNIVERZITA KOMENSKÉHO V BRATISLAVE  
FAKULTA MATEMATIKY, FYZIKY A INFORMATIKY



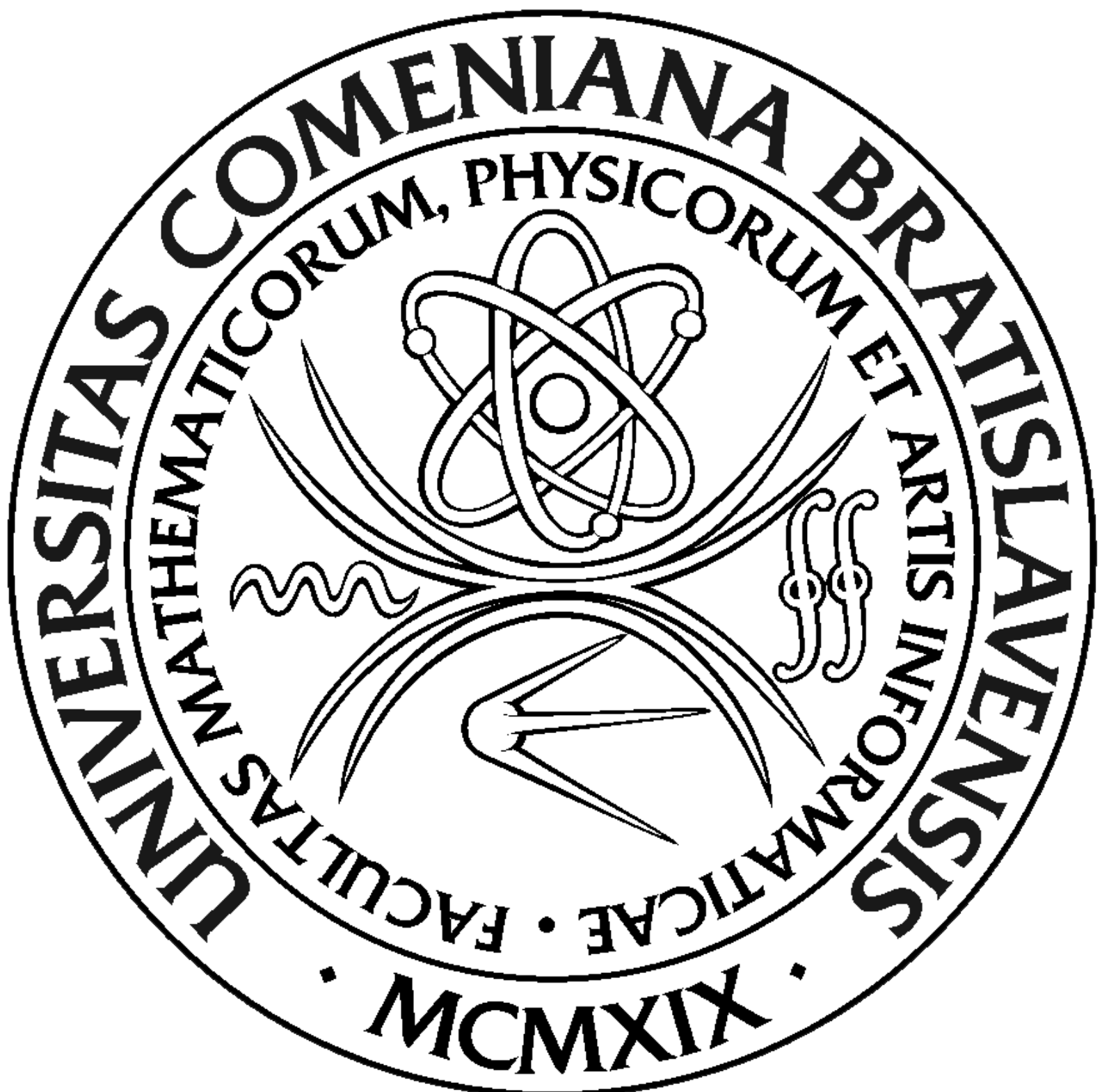
NA EFEKTÍVNE KONŠTRUOVANIE TRACKLETOV OBJEKTOV V

Diplomová práca

Študijný program: Aplikovaná informatika  
Študijný odbor: 2511 Aplikovaná informatika  
Školiace pracovisko: Katedra aplikovanej informatiky  
Školiteľ: prof. RNDr. Roman Ďuríkovič, PhD.

Bratislava, 2017

Bc. Stanislav Krajčovič



Čestne prehlasujem, že túto diplomovú prácu som vypracoval samostatne len s použitím uvedenej literatúry a za pomoci konzultácií u môjho školiteľa.

.....  
Bratislava, 2017

Bc. Stanislav Krajčovič

# Pod'akovanie

Touto cestou by som sa chcel v prvom rade pod'akovať môjmu školiteľovi prof. RNDr. Romanovi Ďuríkovičovi, PhD. za jeho cenné rady a usmernenia, ktoré mi veľmi pomohli pri riešení tejto diplomovej práce. Takisto sa chcem pod'akovať mojím kolegom z YACGS semináru za rady ohľadom implementácie a v neposlednom rade chcem tiež pod'akovať všetkým mojím kamarátom a celej mojej rodine za podporu počas môjho štúdia.

# Abstrakt

Počas astronomických pozorovaní sa získavajú snímky nočnej oblohy, prevažne jej konkrétnej časti, ktoré sa ukladajú do tzv. Flexible Image Transport System (FITS) formátu. Tieto snímky obsahujú signál rôzneho charakteru od šumu spôsobeného elektrickým prúdom a vyčítavaním snímky zo CCD kamier, cez pozadie oblohy až po skutočné objekty ako hviezdy alebo objekty slnečnej sústavy (asteroidy, kométy, vesmírny odpad, atď.). Každý pixel FITS snímky je charakteristický svojou pozíciovou na CCD kamere (x,y) a intenzitou. Tieto údaje sa využívajú na výpočet polohy objektu na CCD snímke a na jeho súhrnnú intenzitu. Na typických astronomických snímkach sa hviezdy javia ako statické body, ktoré možno popísať tzv. rozptylovou funkciou (z ang. Point Spread Function). To neplatí v prípade, keď sa uskutočnia pozorovania vesmírneho odpadu, ktorý sa pohybuje relatívne rýchlo vzhľadom k hviezdnomu pozadiu. V tomto prípade sa objekty javia ako predĺžené čiary a nie ako body. Ak sa počas pozorovaní ďalekohľad pohybuje za objektom vesmírneho odpadu nastáva situácia, že všetky hviezdy sa javia ako predĺžené čiary s rovnakou dĺžkou a smerom, zatiaľ čo snímaný objekt sa javí ako bod. Úlohou študenta/-ky bude naštudovať si literatúru venujúcu sa spracovaniu astronomických FITS snímok, ktoré obsahujú objekty vesmírneho odpadu. Následne študent/-ka navrhne najvhodnejší, alebo aj vlastný algoritmus na segmentáciu snímok, ktorý následne naprogramuje

a otestuje. Počas segmentácie sa identifikujú všetky objekty na snímke a pre každý taký objekt sa vyextrahuje jeho pozícia na CCD snímke (x,y) ako aj súhrná intenzita. Testovanie algoritmu bude uskutočnené na reálnych snímkach na ktorých sa nachádza hviezdne pozadie ako aj vesmírny odpad. Výsledky sa porovnajú s predpoveďami pozícii vesmírneho odpadu, ktoré budú študentovi dodané spolu s reálnymi snímkami získanými ďalekohľadmi na Astronomickom a geofyzikálnom observatóriu v Modre, FMFI UK.

Kľúčové slová: vesmírny odpad, pozorovanie

# Abstract

Keywords: space debris, observation

# Contents

|          |  |           |
|----------|--|-----------|
| <b>1</b> | <b>Introduction</b>  | <b>1</b>  |
| <b>2</b> | <b>Introduction to space debris and observations</b>   | <b>2</b>  |
| 2.0.1    | Small space debris . . . . .   | 4         |
| 2.0.2    | Large space debris . . . . .   | 8         |
| 2.1      | Observations and telescopes . . . . .  | 11        |
| 2.1.1    | ESA OGS . . . . .  | 12        |
| 2.1.2    | FMPI AGO . . . . .   | 13        |
| <b>3</b> | <b>Object dynamics</b>   | <b>16</b> |
| 3.1      | Kepler's laws of orbital motion . . . . .  | 16        |
| 3.2      | Equatorial coordinate system . . . . .   | 17        |
| 3.3      | CCD and image reference frame . . . . .  | 18        |
| 3.4      | Initial orbit determination problem . . . . .  | 18        |
| <b>4</b> | <b>Existing solutions to the problem of tracklet building</b>                                | <b>19</b> |
| 4.1      | k-d trees . . . . .  | 19        |
| 4.1.1    | Efficient intra- and inter-night linking of asteroid de-<br>tectons using kd-trees . . . . . | 20        |
| 4.2      | Uniform linear motion detection . . . . .  | 23        |

|          |  |           |
|----------|--|-----------|
| 4.2.1    | Optical observation, image-processing, and detection<br>of space debris in GEO . . . . . | 23        |
| <b>5</b> | <b>Technical and practical requirements</b>  | <b>25</b> |
| 5.1      | Input data . . . . .   | 25        |
| 5.1.1    | Flexible Image Transport System files . . . . .  | 25        |
| 5.1.2    | .cat files . . . . .   | 29        |
| 5.1.3    | Processing server parameters . . . . .   | 31        |
| <b>6</b> | <b>Proposed solutions</b>  | <b>32</b> |
| 6.1      | Use of linear regression . . . . .   | 32        |
| 6.2      | Use of the Initial Orbit Determination algorithms . . . . .                              | 37        |
| 6.3      | Use of neural network . . . . .  | 38        |
| 6.4      | Hough transform . . . . .  | 38        |
| <b>7</b> | <b>Design and implementation</b>   | <b>39</b> |
| <b>8</b> | <b>Results</b>   | <b>40</b> |
| 8.1      | TDM and MPC formats, CCSDS . . . . .   | 40        |
| 8.1.1    | CCSDS . . . . .  | 40        |
| 8.1.2    | TDM format . . . . .   | 40        |
| 8.1.3    | MPC . . . . .  | 43        |
| 8.1.4    | MPC format . . . . .   | 44        |
| 8.2      | Visualization of results . . . . .   | 45        |
| <b>9</b> | <b>Conclusion</b>  | <b>46</b> |

# Chapter 1

## Introduction

"Space debris" is a term which encompasses both natural and artificial objects and particles. While man-made objects, or "orbit debris", typically orbit around the Earth, meteoroids orbit around the sun and can have trajectories crossing that of the Earth.

There are many risks accompanied by the existence of space debris, namely in-orbit collisions with operational spacecraft, and re-entries. Impacts by millimetre-sized debris could disable a subsystem of an operational spacecraft, debris larger than 1 centimetre would disable the whole spacecraft and debris larger than 10 centimetres would cause catastrophic break-ups. Due to this fact it is important to observe and catalogue debris to prevent collisions with functional man-made satellites and re-entries which could endanger populace.

The aim of this diploma thesis is to develop a comprehensive algorithm and analyse different possible approaches which would identify space debris and extract its position from astronomical CCD images containing observations of star background and unknown objects.

# Chapter 2

## Introduction to space debris and observations

The term space debris encompasses all artificial non-functional objects orbiting around Earth. Each object has different physical properties, such as size and shape and is made of different materials which determine its behaviour and ease of tracking. Usually, in literature, space debris is categorized into five different groups by its type:

1. mission-related debris,
2. fragmentation debris,
3. non-functional spacecraft,
4. rocket bodies,
5. anomalous debris.

Mission-related debris, despite having many different sources and causes, is the most clearly divided between debris released intentionally and unintentionally. Examples of the former are launch adapters, lens covers, and

## *CHAPTER 2. INTRODUCTION TO SPACE DEBRIS AND OBSERVATIONS3*

many other components associated with launch events and payload deployment. The latter category contains protective gloves, cooling liquids, or small particles released from material decay. Common feature of all these objects is that it is a result of a spacecraft's deployment, activation or operation – therefore the term mission-related debris (Klinkrad, 2006).

The polar opposite of mission-related debris is fragmentation debris. As the name indicates, it is composed from objects or particles created during destructive disassociation of a rocket body or an orbital payload and as a result of deterioration when smaller-than-the-parent-object fragments are created. Breakups may be intentional or accidental and are the largest source of catalogued space debris. Products of breakups are ejected into the surrounding area with various initial velocities and spread until they reach the limit of maximum inclination and altitudes of the debris (on the Peaceful Uses of Outer Space. Scientific and Subcommittee, 1999).

Another commonly mentioned type of space debris in various literature is non-functional spacecraft. As of January 2017, there have been 5253 launches of human-made objects into space since the first deployed satellite Sputnik-1 on October 4, 1957 (ESA, 2017). However, a satellite does not have to break into smaller pieces to be considered debris. Functional spacecrafts that reach their end of life are either re-orbited or left in their former orbit. Historically, re-orbiting manoeuvres were performed only in geostationary orbit (GEO, approximately 36 000 kilometres above Earth's equator) and by spacecrafts carrying nuclear material in low Earth orbit (LEO, approximately 2 000 kilometres above Earth's equator), as well as for vehicles with crew and for reconnaissance. Nevertheless, according to the Mitigation Guidelines released in 2002 by Inter-Agency Space Debris Coordination Committee (IADC), spacecrafts in LEO should be allowed to fall into the

atmosphere and burn up within 25 years of mission end and spacecrafts in GEO should be re-orbited at least 300 kilometres above the GEO orbital ring and left in so-called “graveyard orbit”. Satellites in GEO are not lowered because it is not efficient to carry extra fuel specifically for this purpose.

The last category of space debris consists of rocket bodies. Spacecrafts mentioned in the previous section are launched on vehicles which are constructed for this single purpose. Deployment process consists of one or more phases that are represented by rocket bodies. The number of rocket bodies needed for ascent into desired altitude is proportional to the altitude – for example spacecrafts with missions in LEO only need one rocket body while those in GEO need may need up to three. First stages need to have enough thrust to lift the satellite despite gravity and air resistance and are generally bigger than other stages which are used to position the spacecraft in the final steps of deployment. As such, larger rocket bodies usually re-enter into the atmosphere and burn up or fall into the ocean, while the smaller stages are left at various altitudes. This kind of space debris poses danger especially because of its large dimensions and potentially leftover fuel that may cause explosions which produce new fragmentation debris.

### **2.0.1 Small space debris**

The size of space debris varies from particles less than one millimetre small to objects more than one metre large. While the smallest particles are difficult to track, the amount of those that have size less than 1 centimetre is estimated to be more than 170 million (ESA, 2017). Other sources list the population of debris with diameters bigger than 1 mm as  $3 * 10^8$  objects and  $3 * 10^{13}$  objects with diameter bigger than 1  $\mu\text{m}$  (Klinkrad, 2006).

A major source of sub-centimetre reproductive space debris is the effect

of harsh space environment on spacecraft surface materials. Intense UV radiation and atomic oxygen cause decay on spacecraft surfaces usually coated in paint for thermal purposes or other thermal protection materials. Paint flakes, such as in Figure 2.1, created by these processes have small initial velocity and in combination with their relatively small size are not as dangerous to functional satellites though they can cause significant damage. They are categorised as fragmentation or sometimes as anomalous debris.

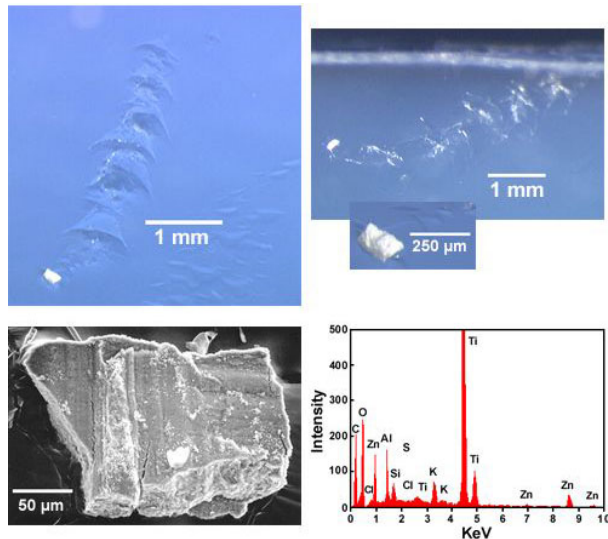


Figure 2.1: Paint flakes captured by Mir Environmental Effects Payload.

Hypervelocity collisions of small debris objects create particles upon impact which are called ejecta and are part of the fragmentation debris group. This type of debris is not detectable from ground and is measured by examining surfaces of space crafts returned to Earth or by dedicated debris detectors situated in LEO altitudes. However, because of the mentioned high speeds of many of these particles, the pressure under which the impact is made is more than 100 GPa and temperatures more than 9000 degrees Celsius (Klinkrad, 2006). As a result of this there is only a little impacting material left on the surface since most of it evaporates. Figure 2.2 shows a hypervelocity impact

## CHAPTER 2. INTRODUCTION TO SPACE DEBRIS AND OBSERVATIONS6

which created a hole in a panel of the Solar Maximum Mission satellite.

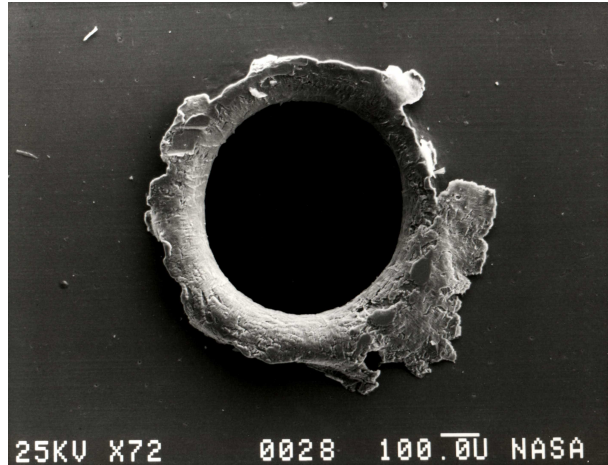


Figure 2.2: A hole made by debris in a solar panel.

While delivering payloads into orbit, burning process of solid rocket motors releases particles called SRM slag and SRM dust which are classified as non-fragmentation, unintentional debris and are composed mainly of aluminium oxide. It is assumed that during 1,032 SRM firings throughout 44 years, or 2,440 up to year 2017 (ESA, 2017), about 1000 tons of propellant was released, 320 tons of which were aluminium oxide particles (SRM dust) and 4 tons SRM slag. Due to orbital perturbations and different sizes, it is estimated that only one ton of SRM dust and three tons of SRM slag remain in the orbit (Klinkrad, 2006). Figure 2.3 shows a piece of SRM slag recovered from a test firing of a shuttle solid rocket booster.

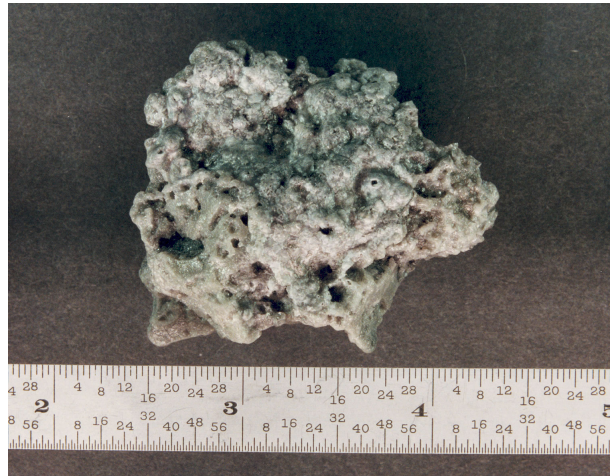


Figure 2.3: SRM slag.

Another similar but rare type is droplets of sodium-potassium alloy (NaK), a coolant in Russian RORSAT (Radar Ocean Reconnaissance Satellites). To the contrary to previous methods used to capture and observe small debris, these particles were detected by ground-based radar and optical measurements in the early 1990s. NaK droplets were used in a particular type of reactor used between October 1970 and March 1988, throughout sixteen launch events. It is estimated that whole of 208 kilograms of NaK coolant was released during this period. Since this kind of reactor is no longer used, NaK droplets along with Westford Needles (see next paragraph) are considered a historic, non-reproducing space debris.

A communications experiment between years 1961 and 1963 consisted of deploying copper wires around the Earth. These copper wires were 1.78 cm long and 25.4  $\mu\text{m}$  in diameter in the first experiment and 17.8  $\mu\text{m}$  in diameter in the second experiment - see Figure 2.4. They were originally encased in rotating containers and supposed to disperse to form a layer of radio frequency reflecting dipoles. However, the dispersion failed and the estimated mass of Westford Needles is less than 60 kg in two clusters.

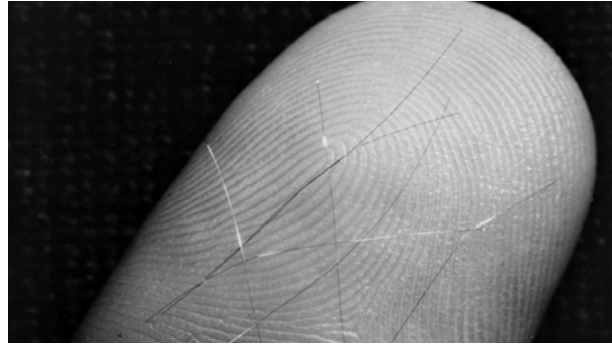


Figure 2.4: Westford needles.

While being the major contributor to the population of space debris, small objects are, as mentioned, virtually unobservable from the ground, only by radars and space-based telescopes positioned on LEO, and therefore are not the main focus of this work. For further information see (Klinkrad, 2006) or (Šilha, 2012).

### 2.0.2 Large space debris

The most extensive database of tracked objects in orbit is maintained by US Space Surveillance Network (USSSN). Only objects which exceed certain sizes at certain altitudes can be tracked with ground-based radar and optical measurements. Due to this, USSSN incorporates only debris larger than 5 cm to 10 cm in LEO and 30 cm to 20 m in GEO (geostationary altitudes, approximately 36,000 km). Currently, USSSN contains more than 42,000 tracked objects with more than half of them still in orbit. About 24% of them are satellites and 18% are spent upper stages and other mission-related objects (ESA, 2017). Out of 175 fragmentation events recorded since 1961 until January 2002, 48 have been categorized as deliberate explosions or collisions, 52 as propulsion system explosions, 10 have been caused by aerodynamic forces, 7 are believed to have been electrical system failures and 1 was an accidental

collision (Klinkrad, 2006).

Deliberate collisions have been caused mainly as test scenarios for Strategic Defence Initiative (SDI) experiment. In the first case, an anti-satellite missile was fired and destroyed Solwind P78-1 satellite. The second collision was between the USA-19 spacecraft and an upper stage used to bring it into the orbit. Number of fragments for both of these events was 285 and 13 respectively but as a result of natural cleaning processes or deliberate planning, from H-10 event only 33 objects were on orbit by January 2002 and from Solwind P78-1 only 2. However, the largest fragmentation event occurred in 2007 when China intentionally destroyed its non-functional weather satellite Fengyun-1C, generating more than 3,215 new fragments.

Even though unintentional collisions are rare and only 0.2% of all catalogued objects until February 2009 have been created in this way it is expected that they will be a major cause for debris in the future. On November 13, 1986 an Ariane-1 H-10 upper stage exploded, causing a fragment cloud containing 488 catalogue entries. The first unintentional in-orbit collision came to pass 10 years later between a French satellite and the mentioned H-10 upper stage explosion fragment. The Cerise satellite was still able to function afterwards and the event caused only one new piece of catalogued debris (Šilha, 2012).

A particularly interesting class of space debris is anomalous debris. It's a specific group that has small velocity and high area to mass ratio (A/M) and its formation process is unknown. The exemplary member of anomalous debris is multilayer insulation (MLI), paint flakes and defunct solar panels. MLI is used as thermal protection to decrease thermal noise on antennae and satellite buses of spacecrafts. MLI can be divided into two types based on their purpose – as a cover/outer layer, and as a reflector/inner layer.

The rapid creation of new debris of non-negligible sizes is a major concern due to the phenomenon called “Kessler syndrome”. The term was coined in 1978 and it means that “each collision would produce several hundred objects large enough to catalogue, increasing the rate that future collision breakups would occur, resulting in an exponential growth in the collision rate and debris population” (Kessler, 2009).

Spent upper stages and non-functional satellites are one of the largest and most compact space debris. Even though many of them re-enter the Earth’s atmosphere on purpose and their life on orbit is relatively short, or are elevated on further orbits, they still pose a threat to functional satellites or missions in progress. Figure 2.5 shows such spent upper stage, specifically Agena D, the most launched American upper stage (Genesis of Agena D, 2006).



Figure 2.5: Agena D upper stage.

## 2.1 Observations and telescopes

Optical telescopes are usually placed at high altitudes, with minimal light pollution and good meteorological and atmospheric conditions. Telescopes used for satellite tracking must be operated at "astronomical night" (Sun being more than 18° under the horizon) while the tracked objects must still be illuminated by the Sun (Klinkrad, 2006).

Telescopes are divided into two groups: refractors and reflectors. The first type uses lens systems to observe objects while the second one uses mirror surfaces to focus incoming light. Reflectors are categorized into four subgroups:

1. Newton telescopes,
2. Cassegrain telescopes,
3. Coudé telescopes,
4. Ritchey-Chrétien telescopes.

The base upon which a telescope is placed is called a mount. As with telescopes, there are many types of mounts with each giving different advantages than the other. Mounts are able to rotate both vertically and horizontally.

A telescope collects photons which are reflected or emitted by a space object. Usually, the origin of photons is the Sun and depending on the angle between the Sun, the object and the observer and reflection efficiency of the target the intensity is determined. The light is then translated into an image which can be viewed by an eyepiece or used to generate an exposure on an Charge-Coupled device (CCD). CCDs are photosensitive and solid-state imaging sensors which convert incoming photons into electric charges

on an array of photodetectors. The time-tagged information coming from the photodetectors can be reconstructed into an image with a varying resolution. High-end systems use CCD which produce images with resolution of up to  $4096 \times 8192$  pixels. CCDs naturally heat up and the danger of thermal noise corruption is mitigated by using active coolants, such as liquid nitrogen (Klinkrad, 2006).

### 2.1.1 ESA OGS

European Space Agency (ESA) Optical Ground Station (OGS) is a Zeiss telescope built in the Teide Observatory, in Tenerife, Spain, 2,400 m above sea level. It's a one metre telescope with focal length 13.3 m originally used for tests with laser link, space debris observation and other astronomical night observations. The CCD camera has a field of  $4000 \times 4000$  pixels. The telescope can detect and track near-GEO objects down to 10-15 cm in size. Throughout years 2009 to 2013 the telescope has been credited by Minor Planet Center (MPC) with discovery of 38 minor planets.

Besides being used for aforementioned astronomical purposes, its unique location and ability to be tilted to near-horizontal position and point at a different station, namely Jacobus Kapteyn Telescope in La Palma, allows it to be employed in quantum telecommunication experiments. The telescope is currently operated by Instituto de Astrofísica de Canarias (IAC).

Figure 2.6 shows the schematic of ESA OGS. One of the most important parts is the Cassegrain focus where the CCD camera is used for observation of asteroids and for long-term monitoring of comets.

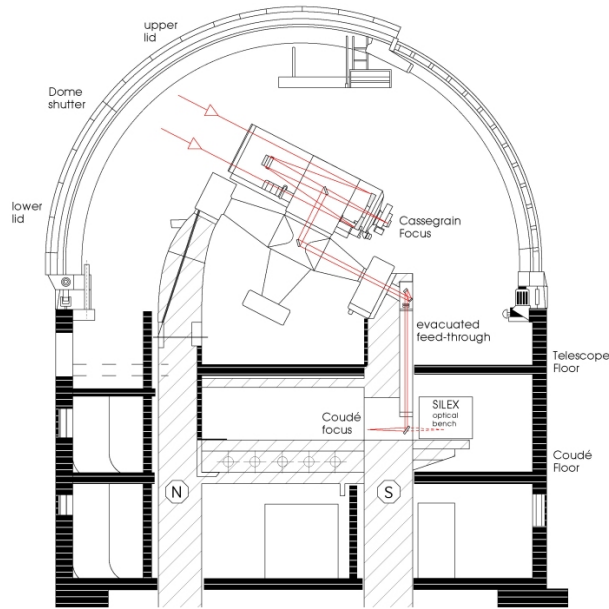


Figure 2.6: ESA OGS schematic.

Figure 2.7 is an image of the Zeiss telescope on an English mount.



Figure 2.7: ESA OGS telescope.

### 2.1.2 FMPI AGO

Astronomické a geofyzikálne observatórium (Astronomical and geophysical observatory, or AGO) is located in Modra, Slovakia and belongs to Fakulta

matematiky, fyziky a informatiky (Faculty of mathematics, physics and informatics of Comenius University, or FMPI). The observatory has a main reflector telescope with a 0.7m Newton design Zeiss telescope with focal length of 2.961m, field of view of  $28.5 \times 28.5$  arc-min on an Equatorial mount. The CCD camera has resolution of  $1024 \times 1024$  pixels.

Figure 2.8 shows the schematic of the main reflector telescope and its position at AGO observatory.

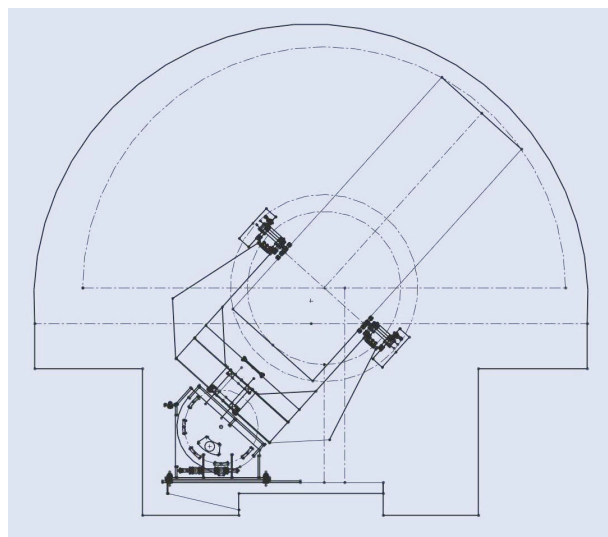


Figure 2.8: Telescope schematic.

Figure 2.9 shows the main telescope which is operated by a computer in the small AGO cupola.



Figure 2.9: The main Zeiss telescope.

# Chapter 3

## Object dynamics

Contents of this chapter

### 3.1 Kepler's laws of orbital motion

Kepler's law of orbital motion describes motion of a satellite in regards to gravitational centre of mass, e.g. Sun to the centre of the galaxy, Earth to Sun, etc. Generally, it states that such motion follows a trajectory which is always elliptically shaped.

In astronomy, an object's position in an inertial system, e.g. geocentric or heliocentric, at specific time (reference epoch  $t$ ) can be defined from two different angles.

Either we define a state vector (three position vector components and three velocity vector components) or we define six orbital elements for an elliptical type of orbit:

- $a$  - semi-major axis [m]
- $e$  - eccentricity [-]

- $i$  - orbital inclination [ $^\circ$ ]
- $\Omega$  - right ascension of ascending node (RAAN) [ $^\circ$ ]
- $\omega$  - argument of pericenter/perigee
- $M_t$  - mean anomaly at reference epoch  $t$  [ $^\circ$ ]

Elements  $a$  and  $e$  define shape of the ellipse while  $i$  and  $\Omega$  define orientation of the elliptical plane,  $\omega$  defines the orientation of the ellipse in the elliptical plane and  $M_t$  defines position of an object on the ellipse. referencia montenbruck chapter 2

## 3.2 Equatorial coordinate system

To describe an object's position on celestial sphere, we use astronomical coordinate system called Equatorial coordinates defined through two parameters, right ascension (RA,  $\langle 0^\circ, 360^\circ \rangle$ ) and Declination (Dec,  $\langle -90^\circ, 90^\circ \rangle$ ). This coordinate reference system is fixed on Earth's equator and vernal equinox (referencia montenbruck). See Figure 3.1 for an illustration of RA/Dec with regards to Earth.

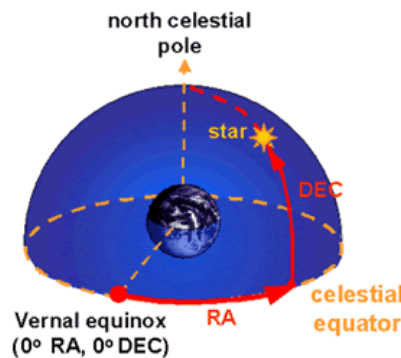


Figure 3.1: RA/Dec illustrated.

### 3.3 CCD and image reference frame

First product of an observation is an object's position in the CCD reference frame ( $x, y$ ). To transform from the  $x$  and  $y$  coordinates to RA/Dec a so called *astrometric reduction* is used which, in general, means linking the two systems together.

The primary goal is to determine the six orbital elements defined in Section 3.1 from RA/Dec in Section 3.2. To confirm that an object is on a conic section we need to find a solution to orbital elements which will yield an elliptical orbit. For more information, see reference .

### 3.4 Initial orbit determination problem

In order to calculate the orbit of object observed with an optical telescope the angle measurements are used (RA/Dec, Section 3.2). To fully determine all six orbital elements we must use at least six parameters - specifically three pairs of angle measurements of the same object. Usually, three pairs of RA/Dec for three different observation epochs, e.g. few minute intervals for satellites.

Methods on how to perform IOD are well defined in the astronomical community - see (referencia montenbruck). The output of this procedure are position vectors or position and velocity vectors for observation epochs. These vectors are then used to determine said orbital elements. (referencia montenbruck)

In the case of observations not being of the same object, some orbital elements will be missing. This characteristic can be used as a filter, or validate gathered data.

# Chapter 4

## Existing solutions to the problem of tracklet building

### 4.1 k-d trees

k-dimensional trees (k-d trees) are a hierarchical data structure that recursively partitions both the set of data points and the space in which they reside into smaller subsets and subspaces. Each node in a k-d tree represents a partial region of the whole space and a set of points contained in the region ()�.

Complexity of k-d trees is similar, or identical in some cases, to other tree data structures. For example, adding a point into a balanced k-d tree takes  $O(\log n)$  time and removing a point from a balanced k-d tree takes  $O(\log n)$  time as well. There are several approaches to constructing a k-d tree, such as finding a median among points (with complexity  $O(n)$ ), sorting all points (with complexity  $O(\log n)$ ) or sorting a fixed number of randomly selected points.

### 4.1.1 Efficient intra- and inter-night linking of asteroid detections using kd-trees

The main focus of the paper is the description of then under development Panoramic Survey Telescope and Rapid Response System (Pan-STARRS) creating the first fully automated Moving Object Processing System (MOPS) in the world. The paper describes the capabilities of the system in areas such as identification of detection of moving objects in our solar system and linking of those detections within and between nights, attributing those detections to catalogued objects, calculating initial and differentially corrected orbits and orbit identification. Further, it illustrates k-d tree algorithms as suitable for linking of objects within and between nights. The paper contains the description of their own pseudo-realistic simulation of the Pan-STARRS survey strategy and shows the results on both simulated and real data sets.

#### Pan-STARRS

The paper describes future goals of Pan-STARRS - obtaining two images per night of each Solar System survey field and using these images to distinguish between real and false detections and to separate stationary and moving transient near-Earth objects (NEOs). The object is obtained and verified across several consecutive nights in order to have high probability of being real and to be able to be submitted to the Minor Planet Center (MPC, see Chapter 8, Section 8.1.3)

#### Pan-STARRS MOPS

Before an image can be processed by MOPS, it must first be processed - cosmic rays and other noise or irrelevant objects need to be removed, it is aligned

and combined into a single image. The resulting image is called "master image" in the paper and is further combined with other master images to create a static-sky image used to produce yet another image containing only transient sources and noise. It is then searched for asteroids and comets pairs of subtracted images are analysed similarly. The preprocessing phase ends with all the identified sources from both images, along with their metadata (time, trail length, axis orientation, flux, etc.), being passed to the MOPS.

The first step, linking intra-night detections of spatially and temporally close objects, which, in addition, have fixed speed among multiple detections, into tracklets, is being done by comparing expected and detected trail length and orientation. Only the objects which pass through this filter are combined into tracklets. The second step is the inter-night linking of tracklets into tracks, which are collections of tracklets. The tracks are verified by IOD (see Chapter 3, Section 3.4) and Orbit Determination (OD, see ()). The complexity of the linking increases like  $\rho^2$ , where  $\rho$  is the number of detections/deg<sup>2</sup>. This can be solved by employing k-d trees to reduce the complexity that increases like  $\rho \log \rho$ .

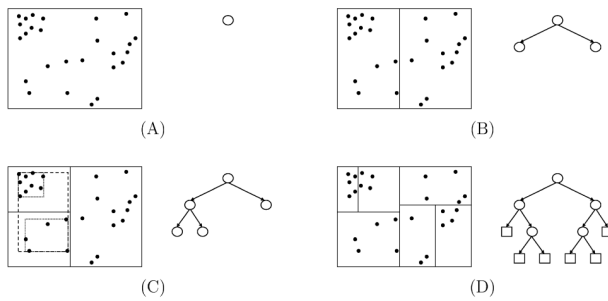


Figure 4.1: k-d tree schematic.

The k-d tree is created from top to down, having full image as the root node. At each level the data in form of points is used to create a bounding

box which is then saved in the corresponding node. The points are then split into two disjoint sets at the widest dimension of the node and bounding boxes are created and assigned again. The recursion is stopped when the currently created node owns less than pre-determined number of points and such node is marked as a leaf node. The construction process is illustrated in Figure 4.1.

Searching for spatially close nodes is done by descending the tree depth first and searching for points within a radius from a given point of query. If the algorithm finds a node that falls out of the radius the algorithm stops because it is guaranteed that each child of the node will fall out of the radius as well. If the algorithm reaches a leaf node, the points in it are tested for the distance from the point of query and eventually added to the results. The algorithm is extended by another constraint - temporal significance. In the paper, they consider each detection as the start of a potential tracklet and look at temporally subsequent detections to judge their relevance and add them to the tracklet. Time is added to the k-d tree as a third dimension. The result of having time as the third dimension is illustrated in Figure 4.2 as a cone which spread is controlled by the maximum allowed speed.

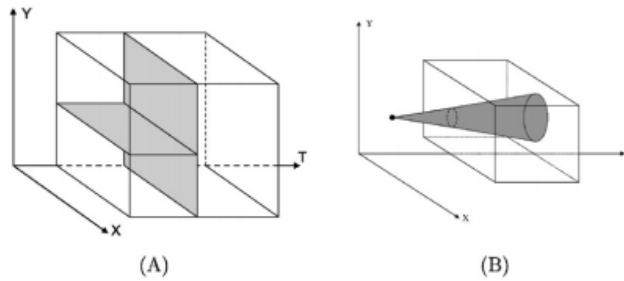


Figure 4.2: k-d tree temporal search.

Inter-night linking is out of scope of this thesis, similarly to creation of synthetic data and their description can be found in the paper - see () .

## 4.2 Uniform linear motion detection

Linear motion is a one dimensional motion along a straight line and mathematically can be explained using one spatial dimension. One of the two types of linear motion is uniform linear motion, which has constant velocity. In the most cases space debris does not follow straight line nor its acceleration is zero. However, when observing under narrow enough field of view (FOV), only part of its trajectory is captured and the object moves according to uniform linear motion.

### 4.2.1 Optical observation, image-processing, and detection of space debris in GEO

The paper describes an efficient detection of space debris on GEO orbit using a telescope with  $3.17^\circ$  FOV producing images with a resolution of  $2048 \times 2048$ . The authors describe image processing and the successive application of the uniform linear motion algorithm to detect objects which are then either matched with the USSTRATCOM catalogue or classified as newly discovered debris.

#### Image processing

The image is preprocessed by subtracting a master dark bias frame from raw images to reduce noise, correcting the sensitivity of pixels and uneven illumination, masking bright pixels and subtracting the sky background frame. Due to the long exposure of 4.7 sec, the stars appear as streaks approximately 13 pixels long and are removed. Noise, such as cosmic rays, do not have diffusive shape and are removed too. The resulting image contains objects that have diffusive shape and are extracted by Gaussian fitting.

### Detection algorithm

The detection algorithm is based on the facts mentioned in Section 4.2 - when we select small enough part of the whole trajectory of an object, the part adheres to the uniform linear motion. After selecting an appropriate candidate from an image (an object having sufficient intensity and correct shape), the next image is considered and only objects that show uniform linear motion and are the brightest are picked. This procedure is repeated until there are 9 positive matches out of 18 light frames and the object is marked as orbital object. See Figure 4.3 for illustration of the detection algorithm.

In conclusion, the algorithm has proven to be effective and efficient and lead to discovery of more than 200 unidentified objects in the span of five nights.

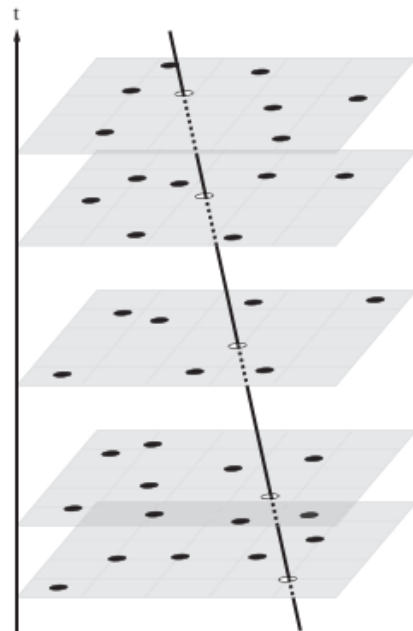


Figure 4.3: Uniform linear motion throughout successive images.

# Chapter 5

## Technical and practical requirements

### 5.1 Input data

Information about potential unknown objects are passed to the program in the form of input files. There are two formats of files which contain relevant metadata, such as right ascension, declination, magnitude, and other, which are vital to the correct functioning of algorithms of tracklet building described in detail in chapter 6.

The first is Flexible Image Transport System (FITS), a standardised and the most commonly used digital file format in astronomy. The second is an output from previous stage of the pipeline, a .cat file.

The formats are described in length in sections 5.1.1 and 5.1.2 respectively.

#### 5.1.1 Flexible Image Transport System files

FITS is the standard archival data format for astronomical data sets.

It was originally designed in year 1981 for transporting image data on magnetic tapes between research institutions. In year 1982, FITS was officially endorsed by International Astronomical Union (IAU) as the format for the interchange of astronomical data.

FITS files in this thesis are used as a source of data about objects and for image stacking (FIT, 2016).

### **File structure**

FITS files consist of three main FITS Structures (structures):

- primary header and data unit (HDU, mandatory)
- conforming extensions (optional)
- other special records (optional).

In our case, all FITS Files contain only the primary HDU which is sometimes referred to as Basic FITS File or a Single Image FITS File.

If used, a structure contains a higher than zero number of FITS Blocks (blocks), each with size of 2880 bytes. Primary HDU always starts with the first block and each following structure begins with a block starting right after the end of the last block of previous structure. Furthermore, the primary HDU and each extension HDU must contain non-zero number of 2880-byte FITS Header (header) blocks, which are mandatory, and an optional array of associated 2880-byte data blocks(FIT, 2016).

### **Data arrays**

If not empty, primary data array has a size of  $1 \times 999$  and is represented by continuous stream of bits. Each data value in the array consists of a fixed

number of bits which are given in the keyword *BITPIX*. If length of data is shorter than length of final block, the difference is filled by setting all the trailing bits to zero (FIT, 2016).

An example of FITS Data array is shown in Figure

## Headers

Headers contain only limited set of text characters encoded in ASCII. Allowed characters are highlighted in Figure 5.1.

| Dec | Bin       | Hex | Char   | Dec | Bin       | Hex | Char  | Dec | Bin       | Hex | Char  | Dec | Bin       | Hex | Char |
|-----|-----------|-----|--------|-----|-----------|-----|-------|-----|-----------|-----|-------|-----|-----------|-----|------|
| 0   | 0000 0000 | 00  | [NULL] | 32  | 0010 0000 | 20  | space | 64  | 0100 0000 | 40  | @     | 96  | 0110 0000 | 60  | `    |
| 1   | 0000 0001 | 01  | [SOH]  | 33  | 0010 0001 | 21  | !     | 65  | 0100 0001 | 41  | A     | 97  | 0110 0001 | 61  | a    |
| 2   | 0000 0010 | 02  | [STX]  | 34  | 0010 0010 | 22  | "     | 66  | 0100 0010 | 42  | B     | 98  | 0110 0010 | 62  | b    |
| 3   | 0000 0011 | 03  | [ETX]  | 35  | 0010 0011 | 23  | #     | 67  | 0100 0011 | 43  | C     | 99  | 0110 0011 | 63  | c    |
| 4   | 0000 0100 | 04  | [EOT]  | 36  | 0010 0100 | 24  | \$    | 68  | 0100 0100 | 44  | D     | 100 | 0110 0100 | 64  | d    |
| 5   | 0000 0101 | 05  | [ENQ]  | 37  | 0010 0101 | 25  | %     | 69  | 0100 0101 | 45  | E     | 101 | 0110 0101 | 65  | e    |
| 6   | 0000 0110 | 06  | [ACK]  | 38  | 0010 0110 | 26  | &     | 70  | 0100 0110 | 46  | F     | 102 | 0110 0110 | 66  | f    |
| 7   | 0000 0111 | 07  | [BEL]  | 39  | 0010 0111 | 27  | '     | 71  | 0100 0111 | 47  | G     | 103 | 0110 0111 | 67  | g    |
| 8   | 0000 1000 | 08  | [BS]   | 40  | 0010 1000 | 28  | (     | 72  | 0100 1000 | 48  | H     | 104 | 0110 1000 | 68  | h    |
| 9   | 0000 1001 | 09  | [TAB]  | 41  | 0010 1001 | 29  | )     | 73  | 0100 1001 | 49  | I     | 105 | 0110 1001 | 69  | i    |
| 10  | 0000 1010 | 0A  | [LF]   | 42  | 0010 1010 | 2A  | *     | 74  | 0100 1010 | 4A  | J     | 106 | 0110 1010 | 6A  | j    |
| 11  | 0000 1011 | 0B  | [VT]   | 43  | 0010 1011 | 2B  | +     | 75  | 0100 1011 | 4B  | K     | 107 | 0110 1011 | 6B  | k    |
| 12  | 0000 1100 | 0C  | [FF]   | 44  | 0010 1100 | 2C  | ,     | 76  | 0100 1100 | 4C  | L     | 108 | 0110 1100 | 6C  | l    |
| 13  | 0000 1101 | 0D  | [CR]   | 45  | 0010 1101 | 2D  | -     | 77  | 0100 1101 | 4D  | M     | 109 | 0110 1101 | 6D  | m    |
| 14  | 0000 1110 | 0E  | [SO]   | 46  | 0010 1110 | 2E  | .     | 78  | 0100 1110 | 4E  | N     | 110 | 0110 1110 | 6E  | n    |
| 15  | 0000 1111 | 0F  | [SI]   | 47  | 0010 1111 | 2F  | /     | 79  | 0100 1111 | 4F  | O     | 111 | 0110 1111 | 6F  | o    |
| 16  | 0001 0000 | 10  | [DLE]  | 48  | 0011 0000 | 30  | 0     | 80  | 0101 0000 | 50  | P     | 112 | 0111 0000 | 70  | p    |
| 17  | 0001 0001 | 11  | [DC1]  | 49  | 0011 0001 | 31  | 1     | 81  | 0101 0001 | 51  | Q     | 113 | 0111 0001 | 71  | q    |
| 18  | 0001 0010 | 12  | [DC2]  | 50  | 0011 0010 | 32  | 2     | 82  | 0101 0010 | 52  | R     | 114 | 0111 0010 | 72  | r    |
| 19  | 0001 0011 | 13  | [DC3]  | 51  | 0011 0011 | 33  | 3     | 83  | 0101 0011 | 53  | S     | 115 | 0111 0011 | 73  | s    |
| 20  | 0001 0100 | 14  | [DC4]  | 52  | 0011 0100 | 34  | 4     | 84  | 0101 0100 | 54  | T     | 116 | 0111 0100 | 74  | t    |
| 21  | 0001 0101 | 15  | [NAK]  | 53  | 0011 0101 | 35  | 5     | 85  | 0101 0101 | 55  | U     | 117 | 0111 0101 | 75  | u    |
| 22  | 0001 0110 | 16  | [SYN]  | 54  | 0011 0110 | 36  | 6     | 86  | 0101 0110 | 56  | V     | 118 | 0111 0110 | 76  | v    |
| 23  | 0001 0111 | 17  | [ETB]  | 55  | 0011 0111 | 37  | 7     | 87  | 0101 0111 | 57  | W     | 119 | 0111 0111 | 77  | w    |
| 24  | 0001 1000 | 18  | [CAN]  | 56  | 0011 1000 | 38  | 8     | 88  | 0101 1000 | 58  | X     | 120 | 0111 1000 | 78  | x    |
| 25  | 0001 1001 | 19  | [EMI]  | 57  | 0011 1001 | 39  | 9     | 89  | 0101 1001 | 59  | Y     | 121 | 0111 1001 | 79  | y    |
| 26  | 0001 1010 | 1A  | [SUB]  | 58  | 0011 1010 | 3A  | :     | 90  | 0101 1010 | 5A  | Z     | 122 | 0111 1010 | 7A  | z    |
| 27  | 0001 1011 | 1B  | [ESC]  | 59  | 0011 1011 | 3B  | :     | 91  | 0101 1011 | 5B  | [     | 123 | 0111 1011 | 7B  | {    |
| 28  | 0001 1100 | 1C  | [FS]   | 60  | 0011 1100 | 3C  | <     | 92  | 0101 1100 | 5C  | \     | 124 | 0111 1100 | 7C  |      |
| 29  | 0001 1101 | 1D  | [GS]   | 61  | 0011 1101 | 3D  | =     | 93  | 0101 1101 | 5D  | ]     | 125 | 0111 1101 | 7D  | }    |
| 30  | 0001 1110 | 1E  | [RS]   | 62  | 0011 1110 | 3E  | >     | 94  | 0101 1110 | 5E  | ^     | 126 | 0111 1110 | 7E  | ~    |
| 31  | 0001 1111 | 1F  | [US]   | 63  | 0011 1111 | 3F  | ?     | 95  | 0101 1111 | 5F  | [DEL] | 127 | 0111 1111 | 7F  |      |

Figure 5.1: Allowed ASCII characters

A header contains at least one header block, each consisting of maximum 80-character keyword sequence. In the 2880-byte block, this puts the maximum number of records at 36. The logical end of the block is marked by the END keyword and if there is space left, it is filled with ASCII character for space.

Keywords are composed of key-value pairs and an optional comment. The presence of the value indicator ('='), ASCII character "equals" followed by

ASCII character for space) determines that the key has a value associated with it. The values field can hold any of the following types:

- character string (eg. '27/10/82')
- logical value (represented as  $T$  or  $F$ )
- integer number (eg. 12)
- real floating-point number (eg. -12.5)
- complex integer number (eg.  $2 + 4i$ )
- complex floating-point number (eg.  $7.8 + 1.7i$ ).

Each FITS file (file) must contain several mandatory keywords (such as *SIMPLE* - describes whether FITS file is a Basic Fits File or not; and other) which are reserved and have fixed types of their values. FITS format also contains reserved keywords that are not mandatory (such as *DATE* - date on which the HDU was created, and other).

In our case, the most relevant keywords are *DATE-OBS* and *EXPTIME*, or *EXPOSURE* in files where the keyword *EXPTIME* is missing (FIT, 2016).

An example of FITS Header is shown in Figure 5.2.

| Header                 | IMAGE  |
|------------------------|--|
| SIMPLE =               | T  |
| BITPIX =               | 16 /8 unsigned int, 16 & 32 int, -32 & -64 real                  |
| NAXIS =                | 2 /number of axes  |
| NAXIS1 =               | 1024 /fastest changing axis                                      |
| NAXIS2 =               | 1024 /next to fastest changing axis                              |
| BSCALE =               | 1.0000000000000000 /physical = BZERO + BSCALE*array_value        |
| BZERO =                | 32768.000000000000 /physical = BZERO + BSCALE*array_value        |
| OBJECT ='              | '  |
| TELESCOP='             | ' / telescope used to acquire this image                         |
| INSTRUME='FLI'         | ' / instrument or camera used                                    |
| OBSERVER='             | '  |
| NOTES ='               | '  |
| DATE-OBS=              | '2017-09-22T18:59:07' /YYYY-MM-DDThh:mm:ss observation start, UT |
| EXPTIME =              | 7.0000000000000000 /Exposure time in seconds                     |
| EXPOSURE=              | 7.0000000000000000 /Exposure time in seconds                     |
| SET-TEMP=              | -40.00000000000000 /CCD temperature setpoint in C                |
| CCD-TEMP=              | -40.00000000000000 /CCD temperature at start of exposure in C    |
| XPIXSZ =               | 24.00000000000000 /Pixel Width in microns (after binning)        |
| YPIXSZ =               | 24.00000000000000 /Pixel Height in microns (after binning)       |
| XBINNING=              | 1 /Binning factor in width                                       |
| YBINNING=              | 1 /Binning factor in height                                      |
| XORGSUBF=              | 0 /Subframe X position in binned pixels                          |
| YORGSUBF=              | 0 /Subframe Y position in binned pixels                          |
| IMAGETYP='Light Frame' | / Type of image  |
| FOCALLEN=              | 0.0000000000000000 /Focal length of telescope in mm              |
| APTDIA =               | 0.0000000000000000 /Aperture diameter of telescope in mm         |
| APTAREA =              | 0.0000000000000000 /Aperture area of telescope in mm^2           |
| SWCREATE=              | 'MaxIm DL Version 5.02' /Name of software that created the image |
| SBSTDVER=              | 'SBFITSEXT Version 1.0' /Version of SBFITSEXT standard in effect |
| FLIPSTAT='             | '  |
| SWOWNER =              | 'Harvester' / Licensed owner of software                         |
| RA =                   | '20:32:55.72' /Image center Ra, solved by Astrometry.net         |
| DEC =                  | '+7:41:13.0' /Image center Dec, solved by Astrometry.net         |

Figure 5.2: FITS Header example

### 5.1.2 .cat files

.cat files are text files generated by the Astrometrica tool accepting FITS files (see 5.1.1) as input, providing interactive graphical user interface to manipulate each FITS file and performs image processing, segmentation, and Astrometrical reduction resulting in an output file with the extension .cat. The astrometrical reduction is performed by constructing centroids, as mentioned in Chapter 3, Section ??.

Detailed description of the contents of a .cat file is in the following subsection.

### Contents of a .cat file

First four lines of a .cat file are a header - first line is empty, second is the name of the column, third contains units in which are values in specific column represented, and fourth is a separator, as shown in Figure 5.3.

| Type | RA    | dRA | Dec.  | dDec | R   | dR  | x | y | Flux | FWHM | Peak | Fit | Designation |
|------|-------|-----|-------|------|-----|-----|---|---|------|------|------|-----|-------------|
|      | h m s | "   | ° ' " | "    | mag | mag |   |   | ADU  | "    | SNR  | RMS |             |

Figure 5.3: .cat header columns

Meaning of each column is as follows:

1. Type - column outlining the type of a detected object; has four valid values:
  - R - a star which has been matched with the star catalogue; if the value is in parentheses, the deviation between the two is too large
  - H - a manually marked object
  - S - a star which has not been matched with the star catalogue
  - ? - an unknown object
2. RA - right ascension in hours/minutes/seconds (see Chapter 3, Section 3.2)
3. dRA - deviation of values of RA between centroid created by Astrometrica and the star catalogue
4. Dec. - declination in degrees/minutes/seconds (see Chapter 3, Section 3.2)
5. dDec - deviation of values of DEC between centroid created by Astrometrica and the star catalogue

6. R - brightness in magnitude
7. dR - deviation of values of brightness between centroid created by Astrometrica and the star catalogue
8. x - position of an object in FITS file on  $x$  axis
9. y - position of an object in FITS file on  $y$  axis
10. Flux - total intensity of all pixels in ADU (analog to digital unit)
11. FWHM - "*full width at half maximum*" describes a measurement of the width of a diffused object
12. Peak - signal to noise ratio; describes the difference between the pixel with the maximal value and background
13. Fit - the deviation of fitting of centroids in image to the star catalogue
14. Designation - an user given input

### 5.1.3 Processing server parameters

The server is a high CPU computer with Linux operating system capable of remote access for multiple users via console or x2goclient. The server is a Supermicro SuperServer 7048R-TR with an Intel® Xeon® E5-2640 v4 with Intel® Turbo Boost Technology, hyper-threading and virtualization capabilities. It also contains 32GB of ECC DDR4 SDRAM 72-bit system memory, 400GB SSD system disk and 4TB SATA 3.0 HDD in RAID1 configuration for additional data storage. 920W power supply and free slots for an additional CPU, system memory sticks and GPUs provide for possible upgrade in the future.

# Chapter 6

## Proposed solutions

Motivated by previous solutions, mentioned in Chapter 4, Sections 4.1.1 and 4.2.1, we propose multiple approaches to solve the problem of tracklet building. The first one, described in Section 6.1 takes advantage of the facts mentioned in Section 4.2.1, specifically that picking sufficiently small part of the object's trajectory will make the object appear as if it moved in uniform linear motion. Section 6.2 describes an algorithm which filters and validates data gathered in Section 6.1. An experimental neural network's construction and relevance is discussed in Section 6.3 and Section 6.4 acknowledges another possible solution which has not been implemented but has been considered nevertheless.

### 6.1 Use of linear regression

Linear regression is a well-known statistical concept modelling the linear relationship between a scalar dependent variable  $y$  and one or more independent variables, usually denoted as  $x$ . In this thesis, we will be using a single scalar predictor variable and a single scalar response variable - simple

linear regression (SLR). We chose SLR because objects in our case appear as if they followed the rules of uniform linear motion (for details on uniform linear motion, see Chapter 4, Section 4.2). For more information about linear regression as a statistical model, see (Freedman, 2005).

To successfully create a tracklet, we need to have three or more confirmed observations out of several images of the same portion of the night sky. As described in Chapter 3, Section ?? all objects are classified beforehand and have several mandatory attributes assigned to them.

As discussed in Chapter 3, Section 3.3 objects' position on the image reference frame in each image in the set of provided inputs (see Chapter 5, Section 5.1) are represented by the values  $x$  and  $y$ . The first draft of linear regression was designed and realised using these values -  $x$  as an independent value and  $y$  as a dependent value.

There are several unidentified or misidentified objects which are potentially the object we are looking for, represented as points.

Firstly, we pair each unidentified point  $p_1$  of an object  $o_1$  from the first image with each unidentified point  $p_2$  of an object  $o_2$  from the second image. Then we create a line  $l$  such that  $p_1, p_2 \in l$ . The final number of existing lines after this initial procedure is equal to  $n_1 * n_2$  where  $n_1$  is the number of unidentified points in the first image and  $n_2$  is the number of unidentified points in the second image. It is important to note that this number might be relatively high depending on the number of unidentified points and therefore on the quality of the pre-processing of each image. If we ignored all fake points we would be left with one line placed among all the real points from the rest of the images.

However, there are several problems. First, fake objects might appear along a line in the same fashion as the real do. Second, the real points might

have non-negligible distance from a line. Third, the first or second point might be deviated too - this would cause the line to have incorrect slope. Fourth, the real points might appear as if their acceleration was non-zero.

The last three problems are mainly caused by atmospheric fluctuations and errors in the CCD camera. We provide solutions to all of these problems in the next paragraph.

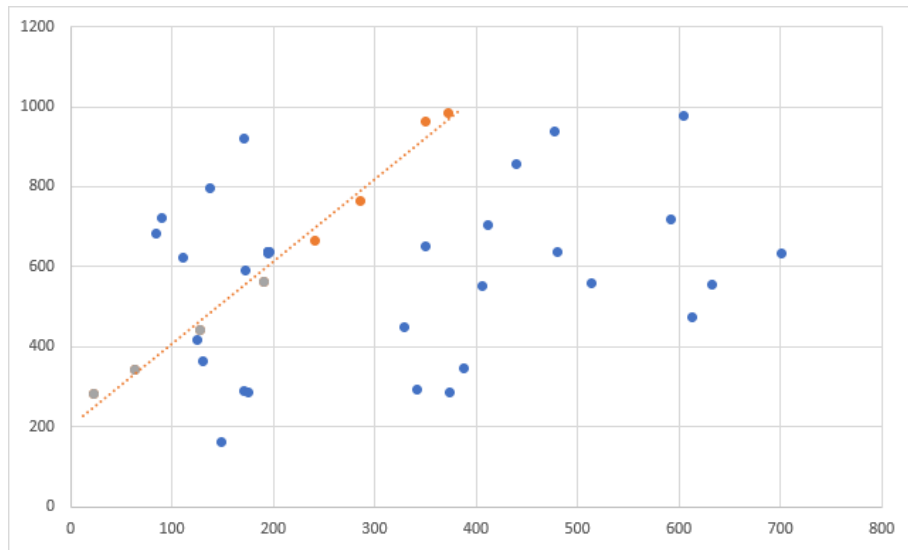


Figure 6.1: Points scattered along a trend line.

Let's imagine we have a single line with points scattered around it, as is illustrated in Figure 6.1. For clarity, the figure shows all points gathered from all images. To further filter out points which have almost zero probability of being real objects we introduce a threshold  $T_l$  which determines a maximum distance a point can have from the line.

The distance of a point  $p = (x, y)$  from the line  $Am + Bn + C = 0$  is calculated by using formula

$$d_p = \frac{|Ax + By + C|}{\sqrt{A^2 + B^2}}$$

We disregard a point if  $d_p > T_l$ , otherwise we process it in the next filter stage. Using only this criterion we can still be left with many false positives and thus, we extend our filter by calculating speed of every considered point.

Speed  $s$  is calculated by using the well-known formula

$$s = \frac{d}{\Delta t}$$

where

$$d = \sqrt{(x_1 - x_2)^2 + (y_1 - y_2)^2}$$

where  $(x_1, y_1)$  and  $(x_2, y_2)$  are two successive points in time and

$$\Delta t = |t_1 - t_2|$$

We get the time  $t_i$ ,  $i \in \langle 1, N \rangle$  where  $N$  is the number of images. We treat first two objects  $o_1$  and  $o_2$  as the baseline - we calculate their speed and then compare speed of each successive object  $o_i$  and choose the one which is closer to the baseline speed.

The last stage of the filter contains calculation of angles between two successive points. Again, consider having two points represented by its positions  $p_i = (x_i, y_i)$ ,  $p_j = (x_j, y_j)$ . We calculate angle  $\theta$  between them as

$$\theta = |\arctan2(y_j - y_i, x_j - x_i)|$$

We then check whether the angle is in a predetermined threshold  $T_a$ . By doing this we create an imaginary 2D cone forming from each point to the plane, as is illustrated in Figure 6.2.

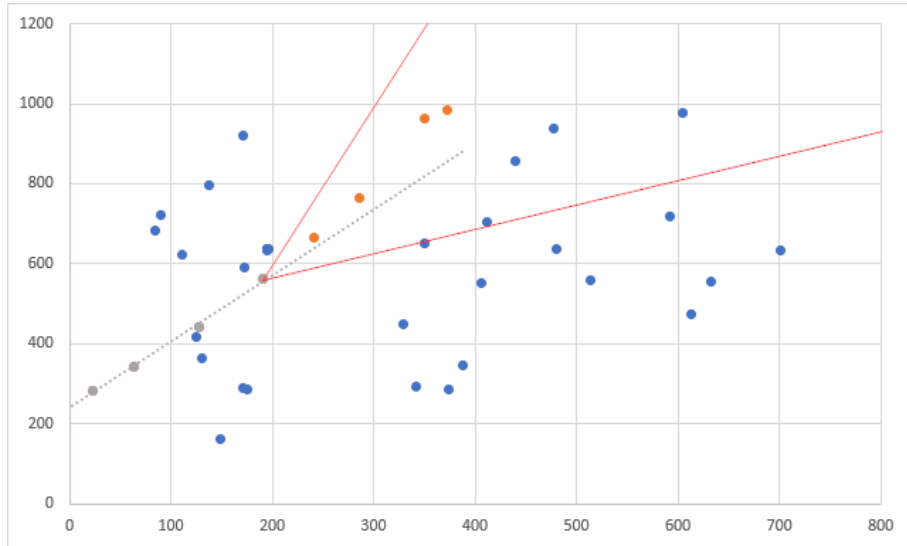


Figure 6.2: Heading of an object.

Only after each of these three filters has been satisfied by the currently chosen object  $o_i$  and its point  $p_i$ , we add it to the list of potential candidates and the SLR is calculated again, containing the last added object as well. It is important to note that we add exactly one object from every image before moving to the next image.

The potential candidates list now contains objects which have a high probability of being real. We touched upon every problem mentioned above - we disregarded points which are too far from the line, we correct the line by dynamically adding objects and re-calculating SLR, we filter out fake objects with nonsense speeds and angles. However, the situation when a fake object passes through all these filters is probable and is remedied by using IOD.

The representation of each object  $o_i$  can be specified either by the standard coordinate system in the two-dimensional Euclidean plane or by a reference system, specifically RA/Dec (see Chapter 3, Section 3.2). The main difference and the reason why we swapped a coordinate system for a reference system is that the RA/Dec is precise and mostly devoid of errors and

deviations. The difference is best shown rather than explained - see Figure 6.3. On the left, there are shown 8 observations of the same object (an asteroid 2017\_PR25), represented in modified RA/Dec and on the right the same 8 observations, represented in the standard coordinate system. It is clearly visible that the deviation of each point in the right graph is more extreme than in the left graph. Acceleration of some of the points appears to be higher than zero - this is because the images were taken in different time intervals.

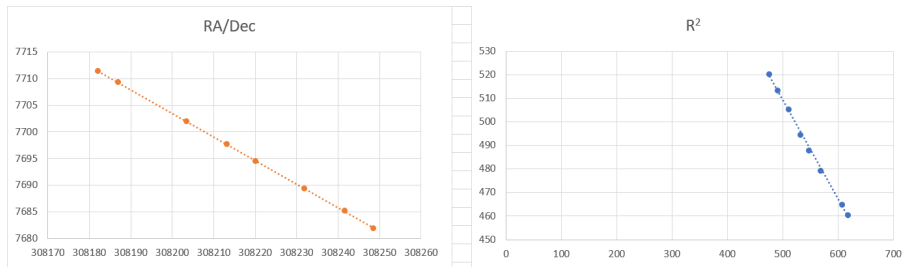


Figure 6.3: RA/Dec comparison.

In order to use RA/Dec in this thesis, we firstly needed to convert original values to degrees. However, due to the nature of the spherical coordinates, the points were only a hundredth, thousandth or even ten thousandth units apart. We had to modify the values by multiplying them by  $10^3$  and therefore dispersing them spatially.

## 6.2 Use of the Initial Orbit Determination algorithms

The theoretical details of IOD are described in Chapter 3, Section 3.4. We used a fully functional implementation of IOD from (Šilha, 2012). For functioning correctly, the algorithm requires longitude and latitude in radians,

altitude (in our case AGO - see Chapter 2, Section 2.1.2) and RA/Dec in radians of three different objects. Then, we perform both Montenbruck and Escobal methods of IOD.

### 6.3 Use of neural network

An experimental part of this thesis is the use of a neural network. We are using a popular framework *tflearn*.

### 6.4 Hough transform

# **Chapter 7**

## **Design and implementation**

# **Chapter 8**

## **Results**

### **8.1 TDM and MPC formats, CCSDS**

This section provides a short insight over standardised output data formats used in this thesis and encouraged by multinational agencies.

#### **8.1.1 CCSDS**

The Consultative Committee for Space Data Systems (CCSDS) is a multi-national forum formed by major space agencies to provide platform for discussion of common problems in the development, operation and maintenance of space data systems and is currently composed of 11 member agencies, 28 observer agencies and over 140 industrial associates (ASRC Federal Technical Services CCSDS, 2017).

#### **8.1.2 TDM format**

Tracking Data Message (TDM) is a standard message format for exchange of spacecraft tracking data between space agencies recommended by the

CCSDS.

TDM consists of lines with text on each line represented by ASCII characters. TDM can be exchanged both in an XML format or a keyword-value notation (KVN) format.

The structure of TDM KVN format has a header and a body and can be divided into three major parts:

- a header
- a metadata section (part of body)
- a data section (part of body).

Data section contains Tracking Data records which hold information about observations. Metadata section and data section added together are called a TDM segment. There is no explicit limit on the number of TDM segments in a body. See Table 8.1 for a more detailed schematic.

Table 8.1: TDM structure

|        |           |            |           |
|--------|-----------|------------|-----------|
| Header |           |            | mandatory |
| Body   | Segment 1 | Metadata 1 | mandatory |
|        |           | Data 1     |           |
|        | Segment 2 | Metadata 2 | optional  |
|        |           | Data 2     |           |
|        | ...       | ...        | optional  |
|        | Segment n | Metadata n | optional  |
|        |           | Data n     |           |

The arrangement of a TDM data section adheres to the KVN format in that it contains records in keyword-value pairs spanning across one line. However, each record has to have a time tag indicating the time associated with the tracking (TDM, 2007).

TDM header contains information that identifies the basic parameters of the message in the KVN format, such as *CREATION\_DATE*, which provides data creation date and time in UTC, or *ORIGINATOR*, which provides information about the file's creator.

The purpose of TDM meta-data's section is to contain configuration details applicable to each TDM data section in the same TDM segment. An example of commonly used metadata keywords are *START\_TIME*, a keyword specifying the starting time of observations, and *STOP\_TIME*, a keyword specifying the ending time of observations in the following TDM data sections.

See Figure 8.1 for a visual example of a TDM file.

```

CCSDS_TDM_VERS = 1.0
COMMENT TDM example created by yyyy-nnnA Nav Team (NASA/JPL)
COMMENT JPL/DSN/Goldstone (DSS-10) weather for DOY 156, 2005

CREATION_DATE = 2005-156T06:15:00
ORIGINATOR = NASA/JPL
META_START
TIME_SYSTEM = UTC
START_TIME = 2005-156T00:03:00
STOP_TIME = 2005-156T06:03:00
PARTICIPANT_1 = DSS-10
DATA_QUALITY = VALIDATED
META_STOP

DATA_START

TEMPERATURE = 2005-156T00:03:00 302.95
PRESSURE = 2005-156T00:03:00 896.2
RHUMIDITY = 2005-156T00:03:00 12.0

TEMPERATURE = 2005-156T00:33:00 304.05
PRESSURE = 2005-156T00:33:00 895.9
RHUMIDITY = 2005-156T00:33:00 11.0

TEMPERATURE = 2005-156T01:03:00 302.55
PRESSURE = 2005-156T01:03:00 895.7
RHUMIDITY = 2005-156T01:03:00 12.0

TEMPERATURE = 2005-156T01:33:00 302.65
PRESSURE = 2005-156T01:33:00 895.7
RHUMIDITY = 2005-156T01:33:00 11.0

TEMPERATURE = 2005-156T02:03:00 301.55
PRESSURE = 2005-156T02:03:00 895.9
RHUMIDITY = 2005-156T02:03:00 11.0

TEMPERATURE = 2005-156T02:33:00 300.45
PRESSURE = 2005-156T02:33:00 895.9
RHUMIDITY = 2005-156T02:33:00 12.0

TEMPERATURE = 2005-156T03:03:00 299.55
PRESSURE = 2005-156T03:03:00 896.1
RHUMIDITY = 2005-156T03:03:00 14.0

TEMPERATURE = 2005-156T03:33:00 298.65
PRESSURE = 2005-156T03:33:00 896.2
RHUMIDITY = 2005-156T03:33:00 15.0

TEMPERATURE = 2005-156T04:03:00 298.05
PRESSURE = 2005-156T04:03:00 896.4
RHUMIDITY = 2005-156T04:03:00 17.0

TEMPERATURE = 2005-156T04:33:00 297.15
PRESSURE = 2005-156T04:33:00 896.8
RHUMIDITY = 2005-156T04:33:00 19.0

TEMPERATURE = 2005-156T05:03:00 294.85
PRESSURE = 2005-156T05:03:00 897.3
RHUMIDITY = 2005-156T05:03:00 21.0

TEMPERATURE = 2005-156T05:33:00 293.95
PRESSURE = 2005-156T05:33:00 897.3
RHUMIDITY = 2005-156T05:33:00 23.0

TEMPERATURE = 2005-156T06:03:00 293.05
PRESSURE = 2005-156T06:03:00 897.3
RHUMIDITY = 2005-156T06:03:00 25.0

DATA_STOP

```

Figure 8.1: TDM format example

### 8.1.3 MPC

Another worldwide organization for Astronomical purposes is the Minor Planet Center (MPC). The organization is in charge of collecting observational data for minor planets, comets and satellites of major planets and

belongs under International Astronomical Union.

### 8.1.4 MPC format

The officially MPC endorsed format is a text file with exactly prescribed form. The format is divided into columns where each column equals one character in a text file. The columns are explicitly set, therefore the format does not contain any headers. There are four kinds of formats - for minor planets, for comets, for natural satellites and for minor planets, comets and natural satellites. In our case, we are using the last type.

The designation for every column is as follows:

- columns 1-12 – designation of observation
- column 14 – NOTE 1 - an alphabetical publishable note (for example *S* for "poor sky", or *K* for "stacked image")
- column 15 – NOTE 2 - indicates how observation has been made (for example *C* for "CCD")
- columns 16-32 – DATE OF OBSERVATIONS - contains the date and time in UTC of the mid-point of observation; the format of this column is "YYYY MM DD.ddddd"
- columns 32-44 – OBSERVED RA - contains observed right ascension; the format of this column is "HH MM SS.ddd"
- columns 45-56 – OBSERVED DECL - contains observerd declination; the format of this column is "sDD MM SS.dd" ("s" for sign)
- columns 57-77 – OBSERVED MAGNITUDE AND BAND - the observed magnitude of an object and band in which the measurement

was made

- columns 78-80 – OBSERVATORY CODE - the code of the observatory in which observation was made (AGO has code 118)

(Minor Planet Center, 2016)

## 8.2 Visualization of results

# Chapter 9

## Conclusion

# Bibliography

- (2007). *Recommendation for Space Data System Standards*. CCSDS Secretariat.
- (2016). *Definition of the Flexible Image Transport System (FITS)*. International Astronomical Union. Version 4.0.
- ASRC Federal Technical Services CCSDS (2017). CCSDS.
- ESA (2017). Space debris: the ESA approach. Brochure.
- Freedman, D. (2005). *Statistical Models: Theory and Practice*. Cambridge University Press.
- Klinkrad, H. (2006). *Space Debris: Models and Risk Analysis*. Astronautical Engineering. Springer.
- Minor Planet Center (2016). MPC format.
- on the Peaceful Uses of Outer Space. Scientific, U. N. G. A. C. and Subcommittee, T. (1999). *Technical report on space debris: text of the report adopted by the Scientific and Technical Subcommittee of the United Nations Committee on the Peaceful uses of Outer Space*. United Nations.
- Šilha, J. (2012). *Identification of the Artificial Objects in Close Vicinity of the Earth*. PhD thesis, Comenius University.